Nanoscale

PAPER

Cite this: *Nanoscale*, 2018, **10**, 1189

Thermo-responsive PNIPAm nanopillars displaying amplified responsiveness through the incorporation of nanoparticles

Juan M. Giussi, *[a] Catalina von Bilderling, [a,b] Emiliano Alarcón,[a] Lía I. Pietrasanta,[b,c,d] Rebeca Hernandez, [e] Rafael P. del Real, [f] Manuel Vázquez,[f] Carmen Mijangos,[e] M. Lorena Cortez [a] and Omar Azzaroni [a]

The possibility of combining more than one stimulus-responsive property into a single material holds interesting potential for the creation of adaptive devices to be used in diverse fields such as drug delivery, nanomedicine and tissue engineering. This paper describes a novel material based on thermo-responsive PNIPAm nanopillars with amplified surface properties through the incorporation of Fe_3O_4 nanoparticles. The incorporation of magnetic nanoparticles into the nanopillars, prepared *via* surface-initiated atom-transfer radical polymerization in anodized aluminum oxide templates, sharply increased their stiffness and hydrophobicity when increasing the temperature above the volume phase transition temperature. Furthermore, their magnetic response turned out to be proportional to the amount of the incorporated nanoparticles. The possibility of sharply increasing the stiffness with a temperature variation close to the human body temperature paves the way to the application of these substrates as "smart" scaffolds for cell culture. Additionally, the presence of superparamagnetic nanoparticles in the nanopillars offers the possibility of using these nanostructured systems for magnetic hyperthermia.

Received 20th August 2017,
Accepted 6th December 2017

DOI: 10.1039/c7nr06209e

rsc.li/nanoscale

Introduction

The surface properties of materials depend on many factors. While the nature of the material is a crucial feature, the correct topographic selection can provide new characteristics to a material and, therefore, enhance – or not – certain properties, such as wettability, adhesion, and rigidity.[1,2]

The surface features of hydrogel-based soft platforms are key players in the development of biomedical materials since their high water content turns them into biocompatible materials.[3] Hydrogel systems have been extensively tested as hosts of a variety of drugs due to their capability to be integrated into specific parts of the human body.[4]

PNIPAm-based hydrogels represent one of the most explored thermo-responsive polymer systems.[5] This system presents a nominal volume phase transition temperature (VPTT) at ~32 °C. Below this temperature, the solvent–polymer interactions become relevant, and, as a consequence, the hydrogel becomes highly hydrated (swollen). Conversely, above the VPTT, the polymer–polymer interactions predominate over the polymer–solvent attractions and the transition results in the water absorbed being expelled from the hydrogel network, which leads to a more compact structure.[6] This transition affects several properties of the material, and translates into multiple applications. Given the fact that mechanical properties can change dramatically, many biocompatible thermo-responsive microgels have been used in several medical fields, such as scaffolding in tissue engineering, drug delivery, nanomedicine, and cell culture.[7–13]

Moreover, nano- and microscale structured hydrogels with a responsive nature have been widely studied as intelligent materials in drug delivery and tissue engineering.[14] It is widely accepted that one of the most versatile methods to nanostructure polymeric materials is through the use of nanoporous anodized aluminum oxide (AAO) templates.[15] Soft nanofibers,[16] nanorods,[17] nanotubes,[18] and nanopillars[19] have

[a]*Instituto de Investigaciones Fisicoquímicas Teóricas y Aplicadas (INIFTA) – Departamento de Química – Facultad de Ciencias Exactas - Universidad Nacional de La Plata – CONICET, 1900 La Plata, Argentina. E-mail: jmgiussi@inifta.unlp.edu.ar; https://www.facebook.com/SoftMatterLaboratory/, https://softmatter.quimica.unlp.edu.ar/*
[b]*Departamento de Física, Facultad de Ciencias Exactas y Naturales, Universidad de Buenos Aires, C1428EHA Buenos Aires, Argentina*
[c]*Instituto de Física de Buenos Aires (IFIBA) – CONICET - Universidad de Buenos Aires, C1428EHA Buenos Aires, Argentina*
[d]*Centro de Microscopías Avanzadas, Facultad de Ciencias Exactas y Naturales, Universidad de Buenos Aires, C1428EHA Buenos Aires, Argentina*
[e]*Instituto de Ciencia y Tecnología de Polímeros, CSIC, Juan de la Cierva 3, 28006 Madrid, Spain*
[f]*Instituto de Ciencia de Materiales de Madrid, CSIC, Sor Juana Inés de la Cruz 3, 28049 Madrid, Spain*

been obtained with homo- and copolymers *via* the infiltration technique on these templates. Nanostructured materials can also be obtained by the synthesis in confinement.[20–22] Inspired by geckos, Cho and Choi[23] fabricated hairy hard poly(dimethylsiloxane) nanopillars with controllable lengths by using AAO templates. With these structures, they were able to obtain a superhydrophobic surface with high adhesion to water.

In previous work, we prepared PNIPAm nanopillars using surface-initiated atom transfer radical polymerization (SI-ATRP) in AAO templates. We have demonstrated that changes in the topological and mechanical properties of PNIPAm nanopillars could occur when acrylamide monomers were incorporated. In contrast to what happens with PNIPAm nanopillars, the stiffness of PNIPAm-AAm nanopillars decreased significantly when the temperature was above the VPTT. Molecular dynamic simulations suggested that, due to the presence of the hydrophilic monomer, a local molecular rearrangement during the volume phase transition could be produced. This rearrangement, involving the local aggregation of NIPAm segments near the centre of the nanopillars and the displacement of the hydrophilic AAm units towards the surface of the nanopillar close to the aqueous environment, led to a decrease in the hydrophilicity of the nanopillars. This behaviour was confirmed *via* contact angle measurements below and above the VPTT.[24]

Additionally, many studies combine PNIPAm systems with inorganic components such as quantum dots,[25,26] silver,[27] gold,[28,29] silica[29] or magnetic nanoparticles[30,31] yielding nanostructured and multifunctional hybrid materials. The combination between the organic and inorganic components establishes a symbiotic relationship in which microgels provide colloidal stability as well as stimuli responsive features, while their inorganic counterparts provide specific properties such as photoluminescence, surface plasmon resonance,[32] or magnetism.[33]

Magnetic-polymeric nanocomposite systems have demonstrated to be of great interest in the design of programmable materials and lab-on-a-chip devices, where the polymers play a key part due to their flexibility, ease of processing, and biocompatibility, among others.[34] To set an example, Drotlef *et al.*[35] prepared magnetic micropatterns with controlled and switchable wettability. They also prepared magnetic micropillars based on polydimethylsiloxane ferrofluid that could be moved in the presence of a magnetic field, producing reversible changes in the surface topography and, consequently, significant changes in the macroscopic surface properties.

This work aims at evaluating the effect of the integration of Fe_3O_4 nanoparticles on the topological and thermo-responsive properties of PNIPAm nanopillars. Additionally, it delves into the magnetic properties of this system. To do so, AAO template confined synthesis was combined with SI-ATRP of NIPAm with *N*,*N*′-methylenebisacrylamide as the crosslinker, in the presence of 10 nm diameter Fe_3O_4 nanoparticles. Scanning electron microscopy confirmed the obtained nanostructures and, through Atomic Force Microscopy (AFM), the topological and mechanical properties of the nanopillars were studied below and above the VPTT. Finally, the magnetic properties of this platform were evaluated using Vibrating Simple Magnetometry (VSM), while the wetting properties were assessed with contact angle measurements. Our investigations yielded a material with amplified mechanical and wetting properties above the volume phase transition temperature of the gel, and a magnetic actuation response proportional to the amount of NPs.

Materials and methods

Materials

N-Isopropylacrylamide (Aldrich, 97%), (3-aminopropyl) triethoxysilane (APTES) (Aldrich 99%), α-bromoisobutyryl bromide (Aldrich, 98%), *N*,*N*′-methylenebisacrylamide (BIS) (Aldrich, 99%), *N*,*N*,*N*′,*N*′,*N*″-pentamethyldiethylenetriamine (PMDTA) (Aldrich, 99%), CuCl (Aldrich, 99.999%), $CuCl_2$ (Aldrich, 99%), phosphoric acid (Aldrich, 85 wt% in H_2O), HCl (Aldrich, 37% in H_2O), and Fe_3O_4 nanoparticles coated with oleic acid (NGAP NP FeO-2205, concentration 100 mg mL^{-1}).

Nanopillar synthesis

Template preparation. Anodized aluminum oxide (AAO) templates were prepared *via* a two-step electrochemical anodization process, as described elsewhere.[36,37] Nanocavities were 200 nm in diameter and 1 μm in length. To carry out TGA and VSM studies, AAO templates with a diameter of 200 nm and a length of 100 μm were used.

Nanopillar preparation. Nanopillars were obtained by surface-initiated atom transfer radical polymerization (SI-ATRP). A number of steps were followed to complete nanopillar synthesis, as previously described by the authors.[24] The grafting of ATRP initiators (silanization and reaction with α-bromoisobutyryl bromide) can be found in the aforementioned paper. The ATRP procedure to obtain the PNIPAm nanopillars, albeit similar, is explained below.

A solution containing 4.70 mmol of NIPAm and 0.11 mmol of BIS was prepared in a mixture of 2 mL of H_2O and 2 mL of MeOH in a Schlenk tube. Then, 0.2, 0.4 and 0.6 mL (5, 10 and 20% with respect to solvent volume) of Fe_3O_4 nanoparticles were added (NP concentration = 0.476, 0.909 and 1.304 w/v %, respectively), in three separate experiments. The tube was submerged in an ice bath and the solution was degassed during 45 min. Then, 0.502 mmol of PMDTA were incorporated and the solution was degassed for 15 min more. Finally, 0.105 mmol of CuCl were added. This mixture, under nitrogen, was sonicated for 5 min and rapidly introduced into an adapted flask with an aminopropylsilane grafted AAO nanoreactor (previously subjected to 5 vacuum and nitrogen cycles of 10 min each). The reaction was carried out for 48 h at room temperature. After this, the AAO nanoreactor with the nanopillars inside was removed from the reaction mixture and thoroughly washed with water. The samples were stored immersed in degassed water in closed containers. Specific treatments were conducted for each study.

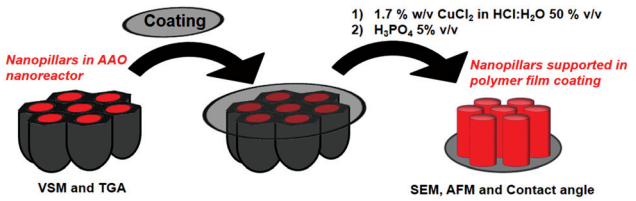

Scheme 1 Sample preparation for each characterization and study. The coatings for SEM and AFM were polymethyl methacrylate films.

Chemical and morphological characterization

In order to characterize the nanosystems by different techniques, the samples were subjected to different treatments, depending on the method used (Scheme 1).

Scanning electron microscopy. The AAO nanoreactor and the nanopillars obtained were morphologically characterized by scanning electron microscopy (SEM) (Philips XL30). In order to perform the analysis of free nanopillars, aluminum was dissolved in a mixture of HCl, $CuCl_2$, and H_2O; and alumina was eliminated in 10 wt% H_3PO_4. Previously, in order to support free nanostructures, a coating was placed on the template (see Scheme 1). The sample was lyophilized before the study so as to preserve morphology.

Thermogravimetric analysis (TGA). The NIPAm nanopillars were characterized by thermogravimetric analysis (TGA) using TGA Q500-TA Instruments. The equipment was kept under a nitrogen atmosphere from room temperature to 700 °C; and gas purge was at 60 ml min^{-1}. The study was performed with the nanopillars inside the alumina template without aluminum; the pore dimensions of the AAO used were 200 nm in diameter and 100 μm in length.

Atomic force microscopy. AFM measurements were performed in an aqueous KCl solution (50 mM) using a Multimode 8 AFM (Nanoscope V Controller, Bruker, Santa Barbara, CA). Peak force tapping (PeakForce-Quantitative NanoMechanics, PF-QNM) was selected as the imaging mode. V-shaped SNML AFM probes (0.07 N m^{-1} cantilever nominal spring constant, 20 nm tip radius, half-open angle of the tip of 19°) were used (Bruker). The spring constants of the cantilevers were determined for each experiment by using the thermal tune method[38] and the deflection sensitivity was determined in fluid using freshly cleaved mica as a stiff reference material. Force curves were acquired using PF-QNM AFM, with a maximum applied loading force of 2.5 nN. From PF-QNM maps, force curves within the surfaces of nanopillars were selected to quantify Young's modulus. The contact point of the force curves was determined according to a published algorithm.[39] The stiffness was obtained using the Oliver and Pharr method,[40,41] through the slope of each curve calculated by performing a linear fit to the upper part of the force curve (between 0.5 nN and 2 nN). The Poisson's ratio was assumed to be 0.5. Image processing was performed using the commercial Nanoscope Analysis software (Bruker). Young's modulus was obtained from force curves through custom written Matlab (Mathworks) routines.

Contact angle. Contact angle measurements were carried out using a Ramé-Hart contact angle system (Model 290) at different temperatures. In a typical measurement, 1 μL droplet of water at a set temperature was deposited on the sample surface. The average contact value was obtained at five different positions of the same sample. The temperatures of the plate and the sample were set at the temperature of each measurement. Scheme 1 shows the sample procedure to determine the contact angle of the nanopillar surface. Contact angle measurements allowed us to determine the wetting surface properties below and above the VPTT.

Vibrating sample magnetometry. The magnetic characterization of the samples was carried out in a vibrating sample magnetometer (VSM), ADE system EV7 KLA-Tencor, under a maximum magnetic field of ±10 kOe, applied parallel (||) to the sample long axis.

Results and discussion

Sample preparation and characterization

AAO nanoreactors, prepared *via* a two-step electrochemical anodization process, were characterized by SEM. Fig. 1 shows the obtained dimensions: 200 nm of pore diameter and ~1 μm of pore length. This figure shows that the nanoporosity of the template is highly regular in size and order, and that the same diameter is maintained all along the pore length.

Fig. 2 shows the micrographs for the Fe_3O_4-PNIPAm nanopillars by the SI-ATRP of NIPAm using BIS as the crosslinker. A micrograph of PNIPAm nanopillars synthesized without nanoparticles is also included. Both nanostructured arrays were fabricated in a 200 nm × 1 μm template.

Fig. 2 shows that nanopillars were formed through SI-ATRP using BIS as the crosslinker in the AAO template, while displaying a peculiar effect: the diameters of the synthesized nanopillars without nanoparticles were comparable to those of the AAO nanoreactors (Fig. 2C), but the size of Fe_3O_4-PNIPAm nanopillars was approximately 300–350 nm (Fig. 2A and B). As it has already been demonstrated, the presence of nanoparticles can decrease the cross-linking degree;[42] and, in this case, this translates into an enlargement of the nanostructures.

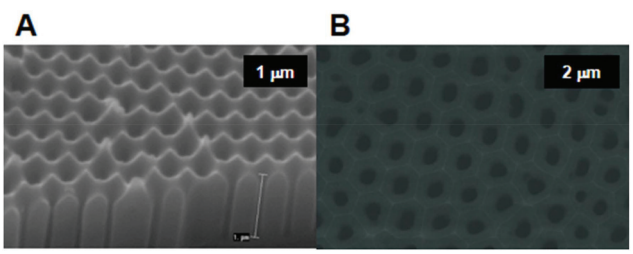

Fig. 1 Morphological characterization of the AAO nanoreactor by SEM. SEM allows us to determine the AAO template diameter and length. The dimensions of the nanoreactor were: ~1 μm (A) of pore length and 200 nm (B) of pore diameter.

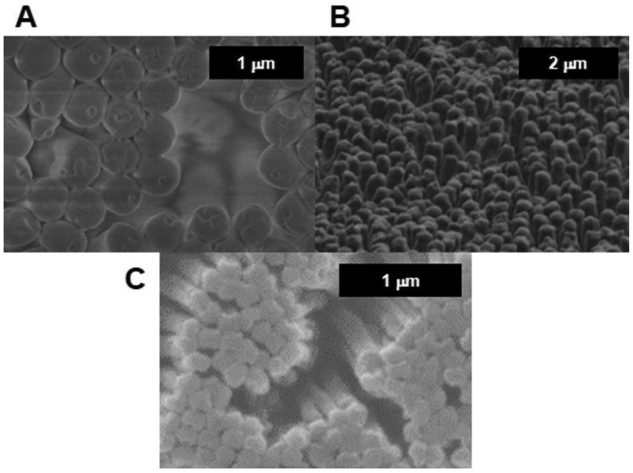

Fig. 2 SEM images of Fe_3O_4-PNIPAm nanopillars: (A) top view and (B) side view; and (C) top view of non-magnetic PNIPAm nanopillars.

After removing the aluminum in $HCl/CuCl_2$ solution, the TGA analysis allowed us to evaluate the degradation profiles and quantify the samples inside the pores. For comparison purposes, the bulk and nanostructured (in confinement) samples of Fe_3O_4-PNIPAm and bulk and nanostructured (in confinement) PNIPAm were run. Fig. 3 shows all the mentioned degradation profiles.

As can be observed in Fig. 3, all TGA profiles show only one thermal event of polymer degradation up to 700 °C. Bulk PNIPAm is completely degraded, while 5% of bulk Fe_3O_4-PNIPAm remains undegraded at this temperature, which could be attributed to the presence of the nanoparticles. The initial degradation temperature for the two bulk samples was the same: 320 °C. On the other hand, the initial degradation temperature for the nanostructured systems was lower: 295 °C for confined PNIPAm and 275 °C for confined PNIPAm with nanoparticles. With regard to confined samples, the alumina template yielded less stability to NIPAm, and the combination of the alumina template and nanoparticles potentiated the degradation effect.

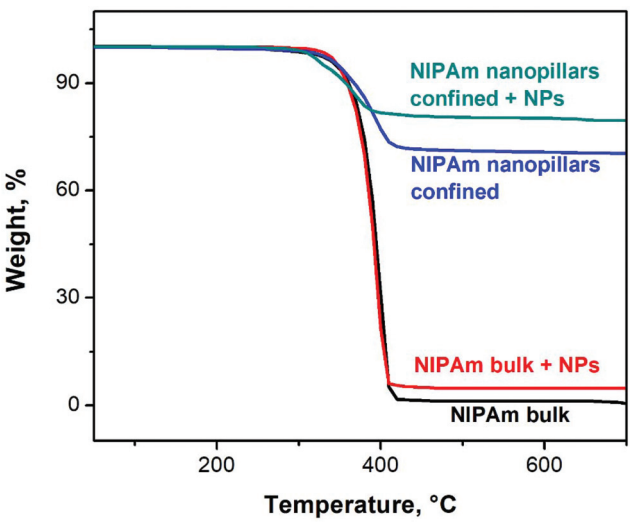

Fig. 3 The TGA profile for bulk and nanostructured (in confinement) Fe_3O_4-PNIPAm; and bulk and nanostructured (in confinement) PNIPAm.

As far as quantity is concerned, confined NIPAm nanopillars degraded to 73 weight%, indicating the presence of 27% NIPAm inside the pores. Confined NIPAm nanopillars with NPs, in turn, degraded to 77 weight%, indicating the presence of 23% NIPAm inside the pores. The remaining 77% corresponds to AAO and NPs. Even though it cannot be ascertained, considering that the presence of nanoparticles does not affect the amount of NIPAm inside the nanocavity, the amount of NPs with respect to dry total mass (AAO + NIPAm + NPs) was close to 15%.

Mechanical properties

Atomic force microscopy (AFM) is proven to be a powerful technique to evaluate the mechanical properties of nanofilms.[43–45] Fig. 4A and B show the *in situ* aqueous AFM topographic images of surfaces of Fe_3O_4-PNIPAm nanopillars below and above the VPTT, respectively. Additionally, Fig. 4C and D show representative AFM force–distance curves and the frequency histograms of the Young's modulus of the nanopillars obtained below and above the VPTT, respectively.

According to our previous work,[24] the stiffness of PNIPAm nanopillars increased from approximately 0.9 MPa to 3 MPa as the solvent temperature did from below to above the VPTT. This can be explained by the rearrangement due to the cross-

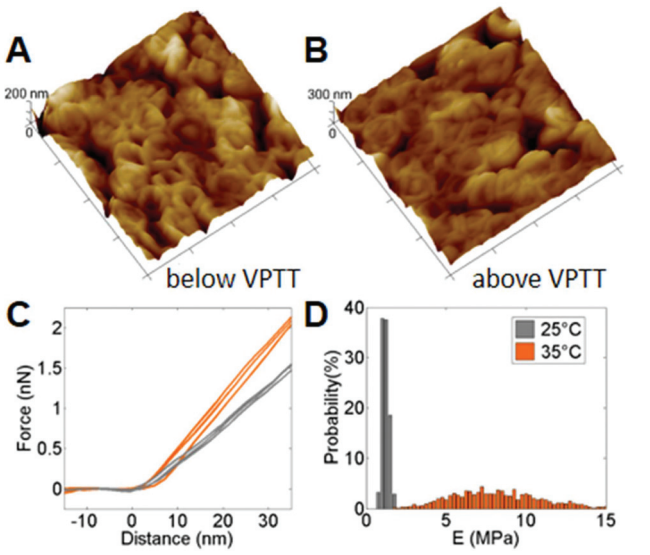

Fig. 4 *In situ* AFM three-dimensional topographic images of the surfaces of Fe_3O_4-PNIPAm nanopillars (A) below and (B) above the VPTT; (C) representative force–distance curves and (D) frequency histograms of Young's modulus at 25 °C (gray, mean stiffness = 1.20 MPa, Std = 0.21 MPa, N = 714 force curves from 8 nanopillars) and 35 °C (orange, mean stiffness = 8.6 MPa, Std = 4.3 MPa, N = 1424 force curves from 8 nanopillars). All images were acquired in solution in PF-QNM mode; scan size: 2 μm × 2 μm, z-scale indicated on each image.

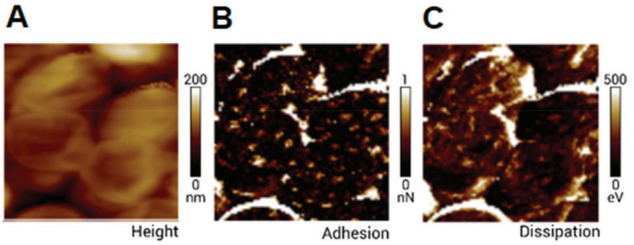

Fig. 5 *In situ* AFM three-dimensional (A) topographic images, (B) adhesion force and (C) dissipation at 35 °C of the surfaces of Fe_3O_4-PNIPAm nanopillars. Scan size: 1 μm × 1 μm.

linked network deswelling at a higher temperature, a process that is accompanied by solvent expulsion. Remarkably, when increasing the temperature, the nanomechanical behavior of Fe_3O_4-PNIPAm nanopillars showed an interesting enhancement of the Young's modulus values. The mean stiffness of Fe_3O_4-PNIPAm nanopillars at 25 °C was 1.20 MPa, a value similar to that of PNIPAm nanopillars without nanoparticles (0.9 MPa); however, at 35 °C, the mean stiffness of Fe_3O_4-PNIPAm nanopillars was 8.6 MPa, a value considerably higher (~3-fold increase) than that of PNIPAm nanopillars without nanoparticles (3 MPa). This interesting amplification suggests that the mechanical properties in the collapsed state of the nanopillars are strongly determined by the presence of the nanoparticles, but the effect of nanoparticles does not seem to play a key role in the swollen state. In the swollen state, the high amount of water inside the nanopillars produces a Young's modulus value similar to that of the nanopillars without nanoparticles. On the other hand, in the collapsed state, water is expelled and the hardness of the nanoparticles begins to have a preponderant role.

The high-resolution AFM nanomechanical images of adhesion force and dissipation further revealed the presence of the nanoparticles in the nanopillars. Fig. 5 shows the topography (A), adhesion force (B) and dissipation (C) at 35 °C of the surfaces of Fe_3O_4-PNIPAm nanopillars. Through adhesion force and dissipation maps, it was possible to detect nanostructured regions within the nanopillar's surfaces. These features, observed also at low temperatures, are allocated to the presence of agglomerated nanoparticles.

Water contact angle

In order to understand and predict the results obtained by SEM and AFM, the surface properties of Fe_3O_4-NIPAm nanopillars were investigated by water contact angle measurements at different temperatures (Fig. 6). These properties were also characterized for PNIPAm nanopillars without NPs. As we have recently shown,[24] PNIPAm nanopillars have an interpenetration effect due to their nanostructured surface, while PNIPAm thin films – obtained by surface-initiated atom transfer radical polymerization from glass – do not. This indicates that the wetting properties of the nanostructured surfaces differ from those of the hydrogel PNIPAm thin films, revealing nanostructured films with higher hydrophilicity due to the interpenetration effect in an aqueous environment.

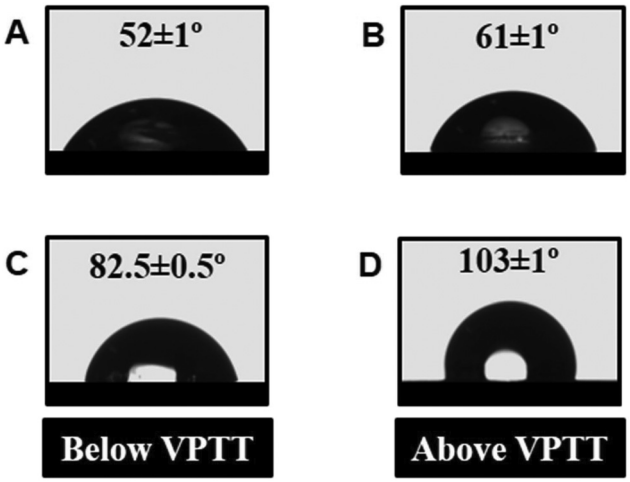

Fig. 6 Contact angle of PNIPAm (A and B, 25 and 35 °C, respectively) and Fe_3O_4-PNIPAm nanopillars (C and D, 25 and 35 °C, respectively), below and above the VPTT. The nanopillars were supported on glass.

If Fig. 6A and C are compared, when the temperature is below the VPTT, the presence of NPs increases surface hydrophobicity. When the temperature is increased above the VPTT, PNIPAm nanopillars without NPs behave as described in the aforementioned paper and the contact angle increases approximately 10°. On the other hand, when the temperature is increased above the VPTT, PNIPAm nanopillars with NPs show an amplified effect with respect to nanopillars without NPs, and the contact angle increases approximately 20°, twice the previous value. The presence of nanoparticles increases the hydrophobicity, probably, due to the coating of oleic acid on the surface of the nanoparticles. As described for mechanical properties, in the swollen state, the concentration of nanoparticles is lower than in the collapsed state. As a consequence, at a high temperature the effect is maximized. As stated in our previous work,[24] the interpenetration effect may have a key part in the amplification of the contact angle at high and low temperatures.

These contact angle results are in agreement with AFM observations: stiffness increases as hydrophobicity does. This observation provides further evidence of the interplay between the mechanical and wetting properties of these nanostructured systems.

Magnetic properties of smart magnetic nanopillars

The magnetic hysteresis loops of the synthesized nanopillars were obtained in a vibrating simple magnetometer, VSM, under a maximum field of 10 kOe applied both in the plane (direction normal to the long axis of the nanopillars) and perpendicular to the samples. Fig. 7 shows the results corresponding to the samples containing concentrations in the order of 0.476, 0.909 and 1.304 w/v % in both directions. The magnetic moment was normalized to the total volume of nano-

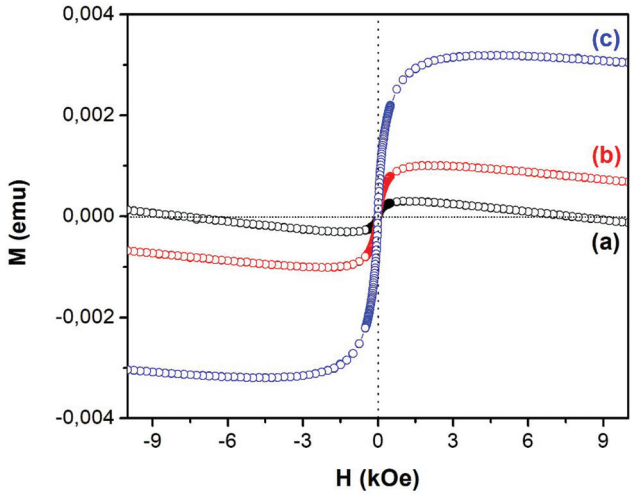

Fig. 7 Magnetic hysteresis loops corresponding to the samples containing concentrations in the order of 0.476 (a), 0.909 (b) and 1.304 (c) w/v % in both directions, plane and perpendicular.

pillars. Overall, the total magnetization of the polymer array increased with the content of nanoparticles. A comparison of the curves obtained in the plane and perpendicular to the samples allows us to observe a higher magnetization of the samples measured in the perpendicular direction.

These results have demonstrated that the prepared nanopillars can be used as a double-responsive nanomaterial – thermal and magnetic. Moreover, the combination of the hardness of nanoparticles and the monomer thermoresponsive properties has potentiated the mechanical and wetting properties. Fe_3O_4-PNIPAm nanopillars show hydrophobicity and amplified stiffness above the transition temperature, characteristics not common in PNIPAm-based hydrogels which turn them into novel and interesting platforms for cell culture substrates and tissue engineering applications. Additionally, the presence of superparamagnetic magnetite nanoparticles provides the possibility of applying these systems for cancer theranostics.[46]

Conclusion

Surface-initiated atom transfer radical polymerization within anodized aluminum oxide templates was used to synthesize a promising thermo- and magnetic-responsive nanostructured substrate based on poly *N*-isopropylacrylamide nanopillars. This nanostructured platform with potential application as a building block for different "smart" substrates presents amplified mechanical and wetting properties above the volume phase transition temperature of the gel network. Our studies revealed that the presence of nanoparticles produced an enlargement of the nanostructures, probably because the nanoparticles decreased the cross-linking degree. On the other hand, TGA analysis allowed us to determine the percentage of nanoparticles with respect to the NIPAm inside the pores.

Concomitantly, AFM analysis revealed that when the temperature was increased above the VPTT, the stiffness of PNIPAm nanopillars also increased. In the case of PNIPAm-Fe_3O_4 nanopillars, though, this increment was especially noticeable. This behaviour was ascribed to a greater compaction of the system with an additional effect due to the presence of the nanoparticles.

The determination of the contact angles below and above the VPTT allowed establishing a correlation between mechanical and wetting properties in this system. When stiffness increased, samples also showed an increase in hydrophobicity. Magnetic characterization confirmed the magnetic actuation of this material due to the presence of Fe_3O_4 nanoparticles, the properties being proportional to the amount of NPs in the gel matrix.

This novel and interesting system based on PNIPAM nanopillars with magnetite nanoparticles could have strong implications in the use and application of thermo-responsive magnetic surfaces in many fields. Moreover, it could be especially important for the molecular design of surface-based platforms for photonics, cancer therapy, tissue engineering, and regenerative medicine, among others.

Conflicts of interest

There are no conflicts to declare.

Acknowledgements

J. M. G, L. C and O. A. acknowledge financial support from the CONICET, the ANPCyT (PICT-2010-2554, PICT-2013-0905, PICT- 2015-0346), the UNLP, Fundación Petruzza and the Austrian Institute of Technology GmbH (AIT–CONICET Partner Group: "*Exploratory Research for Advanced Technologies in Supramolecular Materials Science*" – Exp. 4947/11, Res. No. 3911, 28-12-2011). R. H., C. M, and J. M. G acknowledge the MINECO for its financial support (MAT 2014-53437). R. P. d. R and M. V acknowledge the project NANOFRONTMAG S2013/MIT-2850. J. M. G., C. v. B., L. I. P., M. L. C., and O. A. are staff members of the CONICET.

References

1 H. Assender, *Science*, 2002, **297**, 973–976.
2 Y. Yang, K. Kulangara, R. T. S. Lam, R. Dharmawan and K. W. Leong, *ACS Nano*, 2012, **6**, 8591–8598.
3 M. P. Lutolf, *Nat. Mater.*, 2009, **8**, 451–453.
4 A. Vashist, A. Vashist, Y. K. Gupta and S. Ahmad, *J. Mater. Chem. B*, 2014, **2**, 147–166.
5 M. Kaholek, W. K. Lee, J. Feng, B. Lamattina, D. J. Dyer and S. Zauscher, *Chem. Mater.*, 2006, **18**, 3660–3664.
6 H. Senff and W. Richtering, *J. Chem. Phys.*, 1999, **111**, 1705–1711.
7 J. Peng, T. Qi, J. Liao, M. Fan, F. Luo, H. Li and Z. Qian, *Nanoscale*, 2012, **4**, 2694.

8 J. a. Yang, J. Yeom, B. W. Hwang, A. S. Hoffman and S. K. Hahn, *Prog. Polym. Sci.*, 2014, 1–14.
9 L. Ionov, *Mater. Today*, 2014, **17**, 494–503.
10 D. Wang, D. Cheng, Y. Guan and Y. Zhang, *Biomacromolecules*, 2011, **12**, 578–584.
11 J. Shen, T. Ye, A. Chang, W. Wu and S. Zhou, *Soft Matter*, 2012, 12034–12042.
12 M. Molina, M. Asadian-Birjand, J. Balach, J. Bergueiro, E. Miceli and M. Calderón, *Chem. Soc. Rev.*, 2015, **44**, 6161–6186.
13 N. Becerra, H. Andrade, B. López, L.M. Restrepo and R. Raiteri, *J. Biomed. Mater. Res., Part A*, 2015, **103**, 145–153.
14 S. Ashraf, H. K. Park, H. Park and S. H. Lee, *Macromol. Res.*, 2016, **24**, 297–304.
15 C. Mijangos, R. Hernandez and J. Martin, *Prog. Polym. Sci.*, 2015, **54–55**, 148–182.
16 J. M. Giussi, I. Blaszczyk-Lezak, P. E. Allegretti, M. S. Cortizo and C. Mijangos, *Polymer*, 2013, **54**, 5050–5057.
17 J. Martín and C. Mijangos, *Langmuir*, 2009, **25**, 1181–1187.
18 Y. Wang, J. Y. Lee, H. C. Zeng and K. R. Crescent, *Chem. Mater.*, 2005, **17**, 3899–3903.
19 M. K. Choi, H. Yoon, K. Lee and K. Shin, *Langmuir*, 2011, **27**, 2132–2137.
20 Y. Cui, C. Tao, S. Zheng, Q. He, S. Ai and J. Li, *Macromol. Rapid Commun.*, 2005, **26**, 1552–1556.
21 H. J. Wang, W. H. Zhou, X. F. Yin, Z. X. Zhuang, H. H. Yang and X. R. Wang, *J. Am. Chem. Soc.*, 2006, **128**, 15954–15955.
22 J. M. Giussi, I. Blaszczyk-Lezak, M. S. Cortizo and C. Mijangos, *Polymer*, 2013, **54**, 6886–6893.
23 B. Woo, K. Cho and I. S. Choi, *Adv. Funct. Mater.*, 2008, 1089–1096.
24 B. Sanz, C. von Bilderling, J. S. Tuninetti, L. Pietrasanta, C. Mijangos, G. S. Longo, O. Azzaroni and J. M. Giussi, *Soft Matter*, 2017, **13**, 2453–2464.
25 D. Jańczewski, N. Tomczak, M. Y. Han and G. J. Vancso, *Macromolecules*, 2009, **42**, 1801–1804.
26 R. Gui, X. An, J. Gong and T. Chen, *Mater. Lett.*, 2012, **88**, 122–125.
27 H. Xu, J. Xu, Z. Zhu, H. Liu and S. Liu, *Macromolecules*, 2006, **39**, 8451–8455.
28 T. Kawano, Y. Niidome, T. Mori, Y. Katayama and T. Niidome, *Bioconjugate Chem.*, 2009, **20**, 209–212.
29 H. Jin, X. Liu, R. Gui and Z. Wang, *Colloids Surf., B*, 2015, **128**, 498–505.
30 B. Luo, X.-J. Song, F. Zhang, A. Xia, W.-L. Yang, J.-H. Hu and C.-C. Wang, *Langmuir*, 2010, **26**, 1674–1679.
31 J. Sun, R. Gui, H. Jin, N. Li and X. Wang, *RSC Adv.*, 2016, **6**, 8722–8728.
32 H. Tang, S. Shen, J. Guo, B. Chang, X. Jiang and W. Yang, *J. Mater. Chem.*, 2012, **22**, 16095–16103.
33 L. Borlido, L. Moura, A. M. Azevedo, A. C. a Roque, M. R. Aires-Barros and J. P. S. Farinha, *Biotechnol. J.*, 2013, **8**, 709–717.
34 J. Kim, S. E. Chung, S. Choi, H. Lee, J. Kim and S. Kwon, *Nat. Mater.*, 2011, **10**, 747–752.
35 D. M. Drotlef, P. Blümler, P. Papadopoulos and A. Del Campo, *ACS Appl. Mater. Interfaces*, 2014, **6**, 8702–8707.
36 H. Masuda, M. Yotsuya and M. Ishida, *Jpn. J. Appl. Phys., Part 2*, 1998, **37**, L1090–L1092.
37 M. Hernández-Vélez, *Thin Solid Films*, 2006, **495**, 51–63.
38 J. L. Hutter and J. Bechhoefer, *Rev. Sci. Instrum.*, 1993, **64**, 1868–1873.
39 D. C. Lin, E. K. Dimitriadis and F. Horkay, *J. Biomech. Eng.*, 2007, **129**, 904–912.
40 W. C. Oliver and G. M. Pharr, *J. Mater. Res.*, 1992, **7**, 1564–1580.
41 M. Plodinec, M. Loparic, C. A. Monnier, E. C. Obermann, R. Zanetti-Dallenbach, P. Oertle, J. T. Hyotyla, U. Aebi, M. Bentires-Alj, L. Y. H. Lim and C.-A. Schoenenberger, *Nat. Nanotechnol.*, 2012, **7**, 757–765.
42 L. Castaneda, J. Valle, N. Yang, S. Pluskat, K. Slowinska, L. Castaneda, J. Valle, N. Yang, S. Pluskat and K. Slowinska, *Biomacromolecules*, 2008, **9**, 3383–3388.
43 X. Cheng, H. E. Canavan, M. J. Stein, J. R. Hull, S. J. Kweskin, M. S. Wagner, G. a Somorjai, D. G. Castner and B. D. Ratner, *Langmuir*, 2005, **21**, 7833–7841.
44 S. Schmidt, M. Zeiser, T. Hellweg, C. Duschl, A. Fery and H. Möhwald, *Adv. Funct. Mater.*, 2010, **20**, 3235–3243.
45 A. Burmistrova, M. Richter, M. Eisele, C. Üzüm and R. von Klitzing, *Polymers*, 2011, **3**, 1575–1590.
46 B. Koppolu, Z. Bhavsar, A. S. Wadajkar, S. Nattama, M. Rahimi, F. Nwariaku and K. T. Nguyen, *J. Biomed. Nanotechnol.*, 2012, **8**, 983–990.